Setting-up tunneling conditions by means of Bohmian mechanics

A S Sanz and S Miret-Artés

Instituto de Física Fundamental - CSIC, Serrano 123, 28006 Madrid, Spain

E-mail: asanz@iff.csic.es and s.miret@iff.csic.es

Abstract. Usually tunneling is established after imposing some matching conditions on the (time-independent) wave function and its first derivative at the boundaries of a barrier. Here an alternative scheme is proposed to determine tunneling and estimate transmission probabilities in time-dependent problems, which takes advantage of the trajectory picture provided by Bohmian mechanics. From this theory a general functional expression for the transmission probability in terms of the system initial state can be reached. This expression is used here to analyze tunneling properties and estimate transmissions in the case of initial Gaussian wave packets colliding with ramp-like barriers.

PACS numbers: 03.75.Xp, 07.79.Cz, 03.65.Xp, 03.65.Ta, 82.20.Xr

1. Introduction

Quantum tunneling, the possibility for a system to pass from one state A to another state B *through* an energetic barrier, can be considered as one of the characterizing phenomena of quantum mechanics —although it is more general, appearing whenever a system is described by a wave equation and there is coupling among *evanescent waves* [1], as it happens in optics [2], for example. In 1928, shortly after the formulation of Schrödinger's equation, tunneling was proposed as the physical mechanism that explained both field electron emission [3] and alpha decay [4, 5]. For about 30 years, no satisfactory explanation was possible for these effects, well-known since the end of the XIXth century [6, 7]. Nowadays tunneling not only appears in tunnel microscopy or nuclear physics, but also in other fields, such as semiconductors or catalytic and enzymatic reactions, with important direct applications. There is so much written about tunneling that it seems there is few space left for new conceptual ideas about this phenomenon or mechanism. Nonetheless, it continues stirring our interest.

In the study and analysis of tunneling problems, many different techniques (classical, semiclassical and quantum-mechanical) have been considered in the literature [8, 9]. For example, for low tunneling (i.e., near the top of the barrier), classical and semiclassical approaches, such as the WKB approximation, have been shown to be very appropriate both computationally and interpretively. Actually, after some refinements deep tunneling (i.e., well below the top of the barrier) can also be studied [10]. However, for some other cases, this methodology fails and the problem has to be solved exactly quantum-mechanically. In these cases, though, interpretations are often based on classical and semiclassical arguments. A way

to avoid these thought schemes and provide alternative arguments fully based on quantum-mechanical grounds consists of considering Bohmian mechanics [11,12]. The first work in this direction was developed by Hirschfelder *et al.* [13] in 1974, where tunneling across a two-dimensional square barrier was studied in terms of stationary quantum trajectories or quantum streamlines. As it was shown, under tunneling conditions quantum trajectories present analogous behaviors to those observed in optics in situations such as the frustrated total reflection or the Goos-Hänchen shift. Later on, in 1982, Dewdney and Hiley [14] analyzed the problem of time-dependent scattering off square barriers and wells, formerly considered by Goldberg *et al.* [15] with wave packets. More recently, Lopreore and Wyatt started [16, 17] the development of the so-called *quantum trajectory methods* [18] by studying tunneling through barriers in one and two dimensions. Within this methodological schemes, quantum-mechanical problems are tackled by treating systems as a quantum fluid [19] and then solving the corresponding equations of motion as in classical fluid dynamics. The wave function or any related property is then *synthesized* from trajectory calculations, thus skipping a direct use of the time-dependent Schrödinger equation.

An appealing feature to consider Bohmian mechanics in the study of tunneling dynamics comes from the fact that initial conditions leading to tunneling can be unambiguously determined [16, 17]. This information can be obtained in a rather practical way. For example, it allows us to determine how many trajectories pass the barrier even if at later times they eventually recross it back and forth again (e.g., problems of chemical reaction dynamics [20]). Moved by this fact, here we present an alternative scheme to determine tunneling conditions and estimate transmission probabilities based on Bohmian mechanics. Accordingly, a connection can be established between the transmittance and the system initial state. Thus, first we have considered the time-dependent collision of a Gaussian wave packet with a ramp-like potential, which can be solved analytically. Then, from this model, tunneling properties have been inferred for ramp-like barriers‡, such as those we may find in problems involving electric fields (e.g., electron ionization processes). In particular, a connection between the event-to-event fraction of particles that overcome the barrier and the features characterizing both the initial wave packet (width and momentum) and the barrier (slope) has been determined. Thus, although quantum trajectories are not experimentally observable§, the information extracted from them could be used in a practical fashion in the design or characterization of quantum control experiments involving tunneling (e.g., ionization processes or chemical reactions). In this regard, it is worth mentioning that this idea has also been considered in the literature to determine tunneling times [23] or escape rates for confined multiparticle systems [24].

This work is organized as follows. In section 2, the scheme and hypothesis considered to infer tunneling information from Bohmian trajectories are discussed. In section 3, a practical analysis of this information to estimate transmission probabilities and its check against exact numerical calculations are presented and discussed. Finally, in section 4, the main conclusions extracted from this work as well as its generalization and potential interest in more complex problems are summarized.

‡ In this work, we have only focused on transmission below the barrier height and therefore important problems like above-barrier reflection are not considered. Work related is currently in progress.
§ Recently *photon* paths [21] have been experimentally inferred [22] by using weak measurement processes.

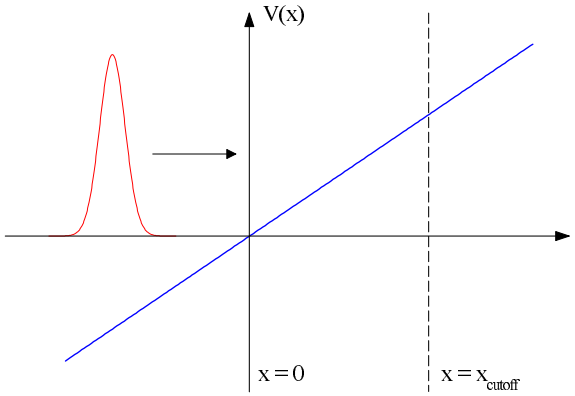

Figure 1. Schematics of the scattering of a Gaussian wave packet with a linear ramp potential. If this potential is truncated at some position $x_{\rm cutoff}$ (i.e., $V(x \geq x_{\rm cutoff}) = 0$), it is shown that tunneling may take place depending basically on how the initial wave packet is prepared and the uphill slope of the resulting barrier (see section 2.3).

2. Tunneling with quantum trajectories

Square barriers are often considered to carry out time-independent analysis of tunneling [25, 26]. However, the collision of a Gaussian wave packet with a ramp-like barrier can be more easily associated with realistic tunneling problems, where the ramp represents to some extent the gradual potential slope met by the wave packet. Thus, apart from containing the physical elements necessary to understand quantum processes and phenomena where tunneling is involved, it is also simple enough to be analytically handled. In this regard, consider the collision of a Gaussian wave packet with a linear ramp-like potential, $V(x) = m\alpha x$, as illustrated in figure 1. At $t = 0$, the wave packet is given by

$$\Psi_0(x) = A_0\, e^{-(x-x_0)^2/4\sigma_0^2 + ip_0(x-x_0)/\hbar}, \tag{1}$$

where $A_0 = (2\pi\sigma_0^2)^{-1/4}$ is the normalization constant, x_0 and p_0 are respectively the (initial) position and momentum of its centroid (i.e., $\langle\hat{x}\rangle = x_0$ and $\langle\hat{p}\rangle = p_0 = mv_0$, with $v_0 \geq 0$), and σ_0 its initial spreading. The ramp has a positive slope along the x-direction (i.e., $\alpha > 0$, since the mass m is always positive). Thus, after colliding with the potential, the wave packet will move backwards with an acceleration $a = -(\partial V/\partial x)/m = -\alpha < 0$. However, if the ramp is truncated at some point $x = x_{\rm cutoff}$ (vertical dashed line in figure 1), tunneling may appear under certain conditions. The purpose below is to determine parameters and conditions leading to this tunneling.

2.1. Scattering with a linear ramp potential

As shown elsewhere [27], the time-evolution of a free Gaussian wave packet like (1) is governed by two dynamical processes: propagation in configuration space and spreading. This fact becomes apparent through the two terms that appear when

computing the corresponding average energy or energy expectation value,

$$\bar{E} = \langle \hat{H} \rangle = \frac{p_0^2}{2m} + \frac{\hbar^2}{8m\sigma_0^2} \equiv \bar{E}_k, \tag{2}$$

where $\hat{H} = \hat{p}^2/2m = -(\hbar^2/2m)\partial^2/\partial x^2$ and $\bar{E}_k$ stands for the free wave packet average kinetic energy. Accordingly, a spreading rate or velocity is defined as $v_s = p_s/m = \hbar/2m\sigma_0$, with p_s being the associated spreading momentum. The dynamical evolution of (1) or any other kind of wave packet regardless of its initial shape (unless it is spreadless [28–30]) is ultimately ruled by the ratio v_0/v_s. This can be easily seen in diffraction problems, where the "shape" of the initial wave function governs its eventual evolution [31–33].

In tunneling processes, the ratio v_0/v_s is also very important. The time-evolution of the Gaussian wave packet (1) colliding with the linear ramp potential of figure 1 can be straightforwardly obtained analytically [34, 35] to yield

$$\begin{aligned}\Psi(x,t) &= A_t\, e^{-(x-x_{\rm cl})^2/4\tilde{\sigma}_t\sigma_0 + ip_{\rm cl}(x-x_{\rm cl})/\hbar + i(p_0^2/2m - m\alpha x_0)t/\hbar - i(p_0 - m\alpha t/3)\alpha t^2/\hbar} \\ &= A_t\, e^{-(x-x_{\rm cl})^2/4\tilde{\sigma}_t\sigma_0 + i[p_{\rm cl}(x - p_0 t/2m) - p_0 x_0 - m\alpha^2 t^3/6]/\hbar},\end{aligned} \tag{3}$$

where $A_t = (2\pi\tilde{\sigma}_t^2)^{-1/4}$ and $\tilde{\sigma}_t = \sigma_0(1 + i\hbar t/2m\sigma_0^2)$. The wave packet (3) evolves in time without changing its Gaussian shape, but only increasing its width as

$$\sigma_t = |\tilde{\sigma}_t| = \sigma_0\sqrt{1 + \left(\frac{\hbar t}{2m\sigma_0^2}\right)^2} = \sigma_0\sqrt{1 + \left(\frac{v_s t}{\sigma_0}\right)^2}. \tag{4}$$

Its propagation follows the classical uniform accelerated motion displayed by its centroid, $x_{\rm cl} = x_0 + v_0 t - \alpha t^2/2$ and $p_{\rm cl} = p_0 - m\alpha t$. As for its average energy,

$$\bar{E} = \bar{E}_k + \bar{V} = \frac{p_{\rm cl}^2}{2m} + m\alpha x_{\rm cl} + \frac{\hbar^2}{8m\sigma_0^2} = \bar{E}_{\rm cl} + \bar{E}_s, \tag{5}$$

where $\bar{V} = m\alpha x_0$. As it is apparent, this expression contains the classical-like term $\bar{E}_{\rm cl}$ accounting for the translation motion and the (quantum-like) spreading energy, $\bar{E}_s$. Since there is no coupling between both motions, these two terms remain constant with time separately. For more complex potential functions, though, this does not hold; the "accommodation" of the wave packet to the corresponding boundary conditions leads to their eventual nonseparability. Nevertheless, their initial separability is enough to infer the long-time dynamics from the earlier stages of the wave packet evolution [36].

Another way to infer the wave packet dynamics is through the probability density associated with (3),

$$\rho(x,t) = \frac{1}{\sqrt{2\pi\sigma_t^2}}\; e^{-(x-x_{\rm cl})^2/2\sigma_t^2}. \tag{6}$$

The centroid of this function evolves along $x_{\rm cl}$, while its width spreads at a rate

$$\frac{d\sigma_t}{dt} = \frac{v_s^2 t}{\sigma_t}. \tag{7}$$

Accordingly, (6) decelerates at a rate $-\alpha$ as it approaches the ramp and accelerates later on again at a rate α after bouncing backwards. The *turning point* (*tp*) for its centroid (the position where $v_{\rm cl} = 0$ and the direction of motion changes) is $x_{\rm tp}^{\rm cl} = x_0 + v_0^2/2\alpha$, reached at $t_{\rm tp}^{\rm cl} = v_0/\alpha$. From (7), we also find that at short times, the spreading increases uniformly, as $\sim (v_s^2/\sigma_0)t$, which indicates an *acceleration* in the wave packet expansion or "boost phase" [16]. Hence, a *spreading* or *boost*

acceleration, $\alpha_s \equiv v_s^2/\sigma_0$, can be defined, which is different from the *dynamical* one, α. In the short-time regime, the wave packet thus spreads as $\sigma_t \approx \sigma_0 + \alpha_s t^2/2$, i.e., undergoing a classical-like uniformly accelerated expansion. On the contrary, in the long-time regime, the spreading rate is constant and equal to v_s, which means a uniform spreading of the wave packet, $\sigma_t \approx v_s t$.

The Bohmian trajectories associated with (3) can be readily obtained after integrating the (quantum) equation of motion [11, 12]

$$\dot{x} = \frac{1}{m}\frac{\partial S}{\partial x} = v_{\rm cl} + \frac{\hbar^2 t}{4m^2\sigma_0^2\sigma_t^2}\,(x - x_{\rm cl}), \tag{8}$$

where $S(x,t) = (\hbar/2i)\ln[\Psi(x,t)/\Psi^*(x,t)]$ is the real-valued phase of Ψ. This yields

$$x(t) = x_{\rm cl} + \frac{\sigma_t}{\sigma_0}\,\delta_0, \tag{9}$$

with $\delta_0 \equiv x(0) - x_0$ being the distance between the initial condition of a quantum trajectory and the centroid initial position. According to (9), the relative distance between any two quantum trajectories x_1 and x_2 increases with time as

$$\frac{x_2(t) - x_1(t)}{x_2(0) - x_1(0)} = \sqrt{1 + \left(\frac{v_s t}{\sigma_0}\right)^2}. \tag{10}$$

That is, in agreement with (7), initially (i.e., short time-scales) the distance between trajectories increases quadratically with time ((10) goes like $\sim \alpha_s t^2/2\sigma_0$), displaying later on a speed-up provoked by the boost acceleration. Nonetheless, at even lager times, the trajectories eventually undergo a slowed-down linear increase with time ($\sim v_s t/\sigma_0$).

2.2. Calculation of transmission probabilities with quantum trajectories

In standard treatments of tunneling [25,26], transmissions are usually determined from matching conditions that the wave function and its first derivative have to satisfy at the barrier edges. However, in a general, non-analytical tunneling problem, transmission probabilities are obtained by computing the quantity

$$\mathcal{T}_\infty \equiv \lim_{t\to\infty} \mathcal{T}(t) = \lim_{t\to\infty} \int_{x_{\rm cutoff}}^{\infty} \rho(x,t)dx \tag{11}$$

where $\mathcal{T}(t)$ is the *restricted probability* [37] in the region behind $x_{\rm cutoff}$. From a Bohmian viewpoint, (11) is statistically computed by considering only those quantum trajectories that reach the region behind the barrier ($x > x_{\rm cutoff}$) or transmission region (i.e., as in a standard classical Monte-Carlo sampling). The initial conditions are randomly distributed according to $\rho_0(x) = |\Psi_0(x)|^2$ and therefore, at any subsequent time, the transmitted trajectories will also be randomly distributed according to the transmitted probability density $\rho_{\mathcal{T}}(x,t) \equiv \rho(x > x_{\rm cutoff}, t)$.

Consider x_2^∞ denotes the asymptotic position of the first trajectory that penetrates into the transmission region and x_1^∞ the position of the last one. These trajectories can then be identified with the conditions that define the beginning and the end of the transmitted part of the wave function at $t \to \infty$. This allows us to reexpress (11) as

$$\mathcal{T}_\infty = \int_{x_1^\infty}^{x_2^\infty} \rho_{\mathcal{T}}(x^\infty)dx^\infty = \lim_{t\to\infty} \int_{x_1(t)}^{x_2(t)} \rho_{\mathcal{T}}(x(t))dx(t), \tag{12}$$

where x^{∞} denotes the position of a quantum trajectory at $t \to \infty$ and confined between x_1^{∞} and x_2^{∞} (i.e., inside the transmission region), $\rho_{\mathcal{T}}(x^{\infty})$ is the probability density evaluated on x^{∞} and dx^{∞} is the distance (at $t \to \infty$) between x^{∞} and a the closest neighbor. The same holds for the expression after the second equality, which stresses the time-dependence of the quantum trajectories and the evaluation of the probability density along them (this is why we have considered explicitly $\rho(x(t))$ instead of $\rho(x,t)$, which simply expresses the probability density evaluated at a point x at a time t). This constitutes a very important step. According to Bohmian mechanics, one can follow the trajectories backwards in time until reaching their initial conditions, i.e., $x_1^{\infty} \to x_1(0)$ and $x_2^{\infty} \to x_2(0)$ as t goes from ∞ to 0. Therefore, (12) can be recast as an integral over initial conditions or, in other words, the initial state of the system, as

$$\mathcal{T}_{\infty} = \int_{x_1(0)}^{x_2(0)} \rho(x(0))dx(0). \tag{13}$$

From this *general* result, we find that the knowledge of both the initial state and the initial conditions $x_1(0)$ and $x_2(0)$, one can already determine the transmission probability (or get an estimate of it) performing the whole dynamical calculation.

In order to illustrate the previous assertion, consider the Gaussian wave packet above. Substituting (9) into (6),

$$\rho(x(t)) = \frac{\sigma_0}{\sigma_t}\,\rho(x(0)), \tag{14}$$

and, after assuming small differentials in (6),

$$dx(t) = \frac{\sigma_t}{\sigma_0}\,dx(0). \tag{15}$$

Then, substituting now (14) and (15) into (12), we obtain (13). This is a rather simple way to analytically proof the validity of this result for the case we are interested in here, namely a Gaussian wave packet (it will be further worked out later on). However, let us stress that (13) it is a general result, which follows from combining the quantum continuity equation and the hydrodynamical picture provided by Bohmian mechanics, and has also a strong connection with the so-called Born rule of quantum mechanics [38] (to some extent, (13) could be considered as a consequence of including time-dependence in Born's rule). Furthermore, despite this physical argumentation, though, a simple analytical proof can also be found which justifies it‖. Consider the Jacobian

$$\mathcal{J} = \frac{\partial x(0)}{\partial x(t)}, \tag{16}$$

from which (14) and (15) can be expressed in a more general way as

$$\rho(x(t)) = |\mathcal{J}|\,\rho(x(0)) \qquad \text{and} \qquad dx(0) = |\mathcal{J}|\,dx(t), \tag{17}$$

respectively. These expressions stress the fact that, as in classical mechanics, in Bohmian mechanics there is also a causal connection (mapping) between two points $x(0)$ and $x(t)$ in configuration space (in classical mechanics this connection is in phase space). Therefore, according to a Liouvillian (conservative) viewpoint, a swarm of initial conditions enclosed within a certain region $\mathcal{C}$ of the configuration space will end up in another bound region $\mathcal{C}'$ of this configuration space at a subsequent time, without

‖ Numerical calculations with general wave packets and barriers have also been carried out to test it, although they are not included in this work.

any loss of trajectories during the evolution. Hence, if the integrated probability in $\mathcal{C}$ (i.e., the total number of trajectories within it) at $t = t_1$ is $P_{\mathcal{C}}(t_1)$ and, at some subsequent time t_2 the integrated probability in $\mathcal{C}'$ is $P_{\mathcal{C}'}(t_2)$, then $P_{\mathcal{C}'}(t_2) \equiv P_{\mathcal{C}}(t_1)$ if the boundary $\mathcal{C}'$ results from the causal evolution of $\mathcal{C}$, i.e., $\mathcal{C} \to \mathcal{C}'$ when $t_1 \to t_2$. Similarly, here we have that (11) and (13) are equivalent regardless of the probability density considered, i.e.,

$$\int_{x_1^\infty}^{x_2^\infty} \rho_{\mathcal{T}}(x^\infty)dx^\infty = \int_{x_1(0)}^{x_2(0)} \rho_{\mathcal{T}}(x(0))dx(0), \tag{18}$$

provided $x_1(0) \to\ x_1^\infty$ and $x_2(0) \to\ x_2^\infty$ as $t : 0 \to \infty$.

The result (13) actually holds for any restricted probability and not only for tunneling transmissions. For example, in problems such as atom-surface scattering [39] or slit diffraction [40], quantum trajectories allow us to determine unambiguously in the initial probability distribution the boundaries that separate the contributions that lead to each specific feature of the corresponding diffraction pattern. More specifically, consider the so-called *peak area intensity*, which is the integral of the probability density covered by a given diffraction peak. In the examples mentioned before, the peak area intensity can be obtained directly from the initial wave function once the two quantum trajectories that delimit a given diffraction peak are known, just by computing the number of (quantum trajectory) initial conditions lying between the initial conditions corresponding to those delimiting trajectories. This is exactly the same problem we face here with respect to tunneling, although instead of dealing with diffraction peak intensities, we have transmission probabilities.

2.3. Tunneling through a linear ramp barrier

In order to estimate transmission probabilities from (13) in the problem we are dealing with here, first the initial conditions for the boundary trajectories have to be determined. In principle, it is reasonable to assume that $x_2(0)$ is such that $\rho_0(x_2(0)) \approx 0$, with $\rho_0(x(0) > x_2(0)) = 0$. Assuming also that ρ_0 must vanish at distances much closer than x_{cutoff}, we can take $x_2(0)$ to infinity for practical purposes. On the other hand, $x_1(0)$ will correspond to some $x_0^{\min}$ that constitutes the onset of transmission, i.e., any trajectory such that $x(0) < x_0^{\min}$ will bounce backwards, thus not passing the barrier. Below, some criteria to estimate $x_0^{\min}$ will be given based on quantum trajectory considerations. For now, these assumptions allow us to analytically approximate (13) by

$$\mathcal{T}_\infty \approx \frac{1}{2}\,\text{erfc}\left(\frac{x_0^{\min} - x_0}{\sqrt{2}\sigma_0}\right), \tag{19}$$

where erfc denotes the *complementary error function* [41]. This is a general result provided the initial state is described by a Gaussian wave packet.

Transmission probabilities can be thus determined from (19) if $x_0^{\min}$ is known or, alternatively, from (13) by means of a random, Monte-Carlo-like sampling of initial conditions, $x_i(0)$, distributed according to ρ_0. Proceeding in this way, (13) becomes

$$\mathcal{T}_\infty \approx \lim_{\mathcal{N}\to\infty} \frac{1}{\mathcal{N}} \sum_{i=1}^{\mathcal{N}} \delta(x_i^{\rho_0}(0) \in (x_0^{\min}, x_2^\infty)), \tag{20}$$

where $\delta = 1$ if the initial condition is contained within the considered spatial range and 0 otherwise —the sampling according to the initial probability density is denoted

by the superscript 'ρ_0'. In the limit of large $\mathcal{N}$, (20) approaches (19), as already seen elsewhere for chemical reactions and atom-surface scattering processes [20, 37].

Below, we provide some considerations based on the ramp barrier from figure 1 to determine $x_0^{\min}$. The cutoff is chosen at a distance such that $\rho_0(x_{\text{cutoff}}) \approx 0$ in order to ensure there is no probability behind the barrier; below, we will assume $x_{\text{cutoff}} = x_0 + N\sigma_0$, without loss of generality, where N is related to some probability onset. Thus, although (9) itself is not a solution of the corresponding tunneling problem, it is very useful in the analysis of tunneling through such barriers in terms of quantum trajectories. Depending on the initial translational motion two cases can be analyzed.

2.3.1. Tunneling dynamics without initial translational motion. When $v_0 = 0$, the wave packet initially rests on the classical turning point and therefore, at any subsequent time, it will slide down the ramp. Appearance of tunneling will then be ruled by which term is dominant in (9), the dynamical down-hill accelerated motion induced by the potential or the wave packet spreading. The former leads the wave packet to move far away from the barrier, while the latter provokes an anti-downhill motion by 'pushing' part of the wave packet opposite to its translation direction.

For the ramp potential, the centroid classical trajectory will evolve backwards (toward $x < 0$) since the very beginning and, in the long-time regime, all quantum trajectories will also move backwards since their dynamics is ruled by α, as seen in (9). Moreover, due to the Bohmian non-crossing rule [27], apparent from (10), the distance among them will increase linearly with time. Thus, the feasibility of tunneling will rely on the dynamical behavior undergone by the ensemble of trajectories starting from x_0 onward (with $\delta_0 > 0$) for their path can be eventually closer to x_{cutoff} and therefore it is likely they tunnel if the boost is strong enough. In brief, a quantum trajectory will undergo tunneling if its *turning point* satisfies the condition $x_{\text{tp}} \gtrsim x_{\text{cutoff}}$.

The turning point of a quantum trajectory is given by a vanishing of its associated velocity (8), i.e., when the translation and spreading terms in this relation cancel each other, making the corresponding (quantum) trajectory to bend over and evolve backwards. Equating the left-hand side of (8) to zero, substituting (9) and $v_0 = 0$ into its right-hand side, and then solving for t the resulting expression eventually yields

$$t_{\text{tp}} = \frac{\sigma_0}{v_s}\sqrt{\left(\frac{v_s}{\sigma_0}\right)^4\left(\frac{\delta_0}{\alpha}\right)^2 - 1} = \frac{\sigma_0}{v_s}\sqrt{\left(\frac{\alpha_s}{\alpha}\right)^2\left(\frac{\delta_0}{\sigma_0}\right)^2 - 1}. \tag{21}$$

This turning time is given as a function of three parameters: (1) the slope of the potential or, in other words, the dynamical acceleration that it imprints on (quantum) particles; (2) the initial spreading of the wave packet, which is a measure of its size at the "preparation" instant and, therefore, can be somehow controlled experimentally; and (3) the initial distance between the corresponding particle and the center of the wave packet, this distance being inconceivable from the viewpoint of standard quantum mechanics.

Given α and σ_0, the question is then whether a particle can cross to the other side of the barrier or not. This information can be extracted from δ_0 as follows. It is apparent from (21) that, in order to observe a "true" turning point (i.e., the particle moves forward for a while before getting backwards), the condition

$$\delta_0 > \left(\frac{\alpha}{\alpha_s}\right)\sigma_0 \equiv \delta_0^c \tag{22}$$

must be fulfilled, where we call δ_0^c the *critical distance* —equivalently, $x(0) > x_c(0) \equiv x_0 + \delta_0^c = x_0 + (\alpha/\alpha_s)\sigma_0$. From this position onwards, all trajectories will display a turning point different from the origin (see section 3), while for any trajectory with $\delta_0 \leq \delta_0^c$ its own initial position $x(0)$ is also its turning point. The trajectory for which $\delta_0 = \delta_0^c$ plays the role of a *separatrix* or *boundary* between two different dynamical behaviors. Note that δ_0^c grows very rapidly with σ_0 ($\sim \sigma_0^4$), which means that the larger the initial spreading, the further away the position of the turning point. In other words, turning points will appear close to x_0 in cases of fast-boosting initially-prepared states, while they will appear far away (even in regions where $\rho \approx 0$) for slow-boosting states.

The position of the turning point for any trajectory with initial condition satisfying (22) is determined by substituting (21) into (9), which yields

$$x_{\rm tp} = x_0 + \frac{\alpha}{2}\left(\frac{\sigma_0}{v_s}\right)^2 + \frac{1}{2}\left(\frac{v_s}{\sigma_0}\right)^2 \frac{\delta_0^2}{\alpha} = x_0 + \frac{\sigma_0}{2}\frac{\alpha}{\alpha_s} + \frac{1}{2}\frac{\alpha_s}{\alpha}\frac{\delta_0^2}{\sigma_0}. \qquad (23)$$

Note that for $\delta_0 = \delta_0^c$ we obtain $x_{\rm tp} = x_c(0)$, which is the initial position for the boundary trajectory. In order to estimate now which initial positions will lead more likely to tunneling, we assume they must be close enough to $x_{\rm cutoff}$. Thus, equating (23) to $x_{\rm cutoff}$ and the solving the resulting equation for δ_0, we find $\delta_0^{\rm min} = (2\alpha\sigma_0/\alpha_s)^{1/2}[x_{\rm cutoff} - x_0 - (\sigma_0\alpha/2\alpha_s)]^{1/2}$, which means that at least all trajectories started from

$$x_0^{\rm min} = x_0 + \sqrt{\frac{2\alpha\sigma_0}{\alpha_s}}\sqrt{x_{\rm cutoff} - x_0 - \frac{\sigma_0}{2}\frac{\alpha}{\alpha_s}} \qquad (24)$$

onward are going to display tunneling through the barrier. Like $x_c(0)$, $x_0^{\rm min}$ also marks the starting point of another type of boundary trajectory: a trajectory that sets up a difference between those with turning points going beyond $x_{\rm cutoff}$ and those that cannot reach this point.

2.3.2. Tunneling dynamics with initial translational motion. From (9), when $v_0 \neq 0$ the wave packet moves towards the ramp and then bounces backwards (its centroid turns at $t_{\rm tp}^{\rm cl} = v_0/\alpha$, when it is at $x_{\rm tp}^{\rm cl} = x_0 + v_0^2/2\alpha$). Again, only those trajectories with $\delta_0 > 0$ will have a chance to cross. Nonetheless, now the initial translational velocity introduces a new control parameter into the barrier passage process, as seen if we substitute (9) into (8), with $v_0 \neq 0$, and then equate to zero the left-hand side, which renders

$$0 = v_0 - \alpha t + \frac{\alpha_s\delta_0}{\sigma_t}\, t. \qquad (25)$$

Unlike the case discussed in Section 2.3.1, here $v_0 \neq 0$ constitutes a second element that can enhance tunneling. Equation (25) can be solved for t by using different techniques employed to solve quartic [42] and cubic [43] equations and different cases can be discussed (depending on the value of the several parameters involved in it).

First, consider σ_0 is relatively large and therefore there is a relatively slow boosting phase. More specifically, the wave packet spreading is assumed to be negligible approximately up to $t \sim t_{\rm tp}^{\rm cl}$, which implies a relatively small boost acceleration compared with α. Under this condition, a first-order expansion in time of (25) renders

$$0 \approx v_0 - \alpha t + \frac{\alpha_s\delta_0}{\sigma_0}\, t, \qquad (26)$$

from which we find

$$t_{\rm tp} = \frac{v_0}{\alpha - \alpha_s \, \dfrac{\delta_0}{\sigma_0}}. \tag{27}$$

Of course, this expression is only valid if $\sigma_t \approx \sigma_0$ or v_0 is relatively large (in the limit $v_0 \to 0$, it does not approach the slow-boosting limit of (21)). Equation (27) can be further simplified to

$$t_{\rm tp} \approx \frac{v_0}{\alpha}\left(1 + \frac{\alpha_s}{\alpha}\frac{\delta_0}{\sigma_0}\right) = t_{\rm tp}^{\rm cl} + t_{\delta_0} \tag{28}$$

if the second term in the denominator of (27) is very small in comparison with α (e.g., for trajectories very near the center of the wave packet, for which δ_0 can also be small). Under this assumption, according to (28), the turning time increases linearly with δ_0. Furthermore, since $\sigma_t \approx \sigma_0$, it can be shown that quantum trajectories will be essentially parallel to the centroidal one,

$$x_{\rm tp} \approx x(0) + (x_{\rm tp}^{\rm cl} - x_0) = \delta_0 + x_{\rm tp}^{\rm cl}. \tag{29}$$

Therefore, for large σ_0 (slow boosting), we have $\delta_0^{\rm min} = x_{\rm cutoff} - x_0 - v_0^2/2\alpha$ and therefore

$$x_0^{\rm min} = x_{\rm cutoff} - v_0^2/2\alpha. \tag{30}$$

That is, regardless of the value of σ_0, there is always an onset of tunneling provided the translational velocity is large enough that the trajectory reaches the ramp cutoff.

The second case is that of fast boosting, i.e., when the initial boosting phase occurs much earlier than the trajectory reaches its turning point. Assuming $\sigma_t \approx v_s t$ and then substituting this into (8) leads to

$$0 \approx v_{\rm eff} - \alpha t, \tag{31}$$

where $v_{\rm eff} = v_0 + v_s\delta_0/\sigma_0$ is an effective constant velocity encompassing both the translational and the spreading velocities, and proportional to δ_0. After (31), a quantum trajectory reaches its turning point at

$$t_{\rm tp} = \frac{v_{\rm eff}}{\alpha} = t_{\rm tp}^{\rm cl} + t'_{\delta_0}, \tag{32}$$

with $t'_{\delta_0} = (v_s/\alpha\sigma_0)\delta_0$. As for the turning-point position, we find

$$x_{\rm tp} = x_0 + \frac{v_{\rm eff}^2}{2\alpha}, \tag{33}$$

which looks pretty much like the expression for the classical turning point, but with v_0 substituted by $v_{\rm eff}$. From (33), we obtain $\delta_0^{\rm min} = (2\alpha\sigma_0/\alpha_s)^{1/2}(x_{\rm cutoff} - x_0)^{1/2} - v_0\sigma_0/v_s$ and therefore

$$x_0^{\rm min} = x_0 + \sqrt{\frac{2\alpha\sigma_0}{\alpha_s}}\,\sqrt{x_{\rm cutoff} - x_0} - \frac{v_0}{v_s}\,\sigma_0. \tag{34}$$

The first part in this relation coincides with (24) in the limit $x_{\rm cutoff} - x_0 \gg \sigma_0\alpha/2\alpha_s$. Hence, in the limit $v_0 \to 0$, both cases will approach. The interest on (34) relies on the fact that, unlike (24), if the spreading rate is not enough to overcome $x_{\rm cutoff}$, there is an extra (translational) energy which may help to surmount the barrier, this favoring the passage. The starting point of the quantum trajectory can then be further away from the barrier cutoff because of the extra velocity.

3. Numerical results

3.1. Parametric study of the transmission probability

In figure 2 we show some calculations¶ of transmission probabilities, $\mathcal{T}_\infty$, as a function of different parameters in order to illustrate the concepts introduced above. Without loss of generality, we have considered $v_0 = 0$, which allows us to better understand the tunneling dynamics "clean" of possible contributions coming from the kinetic energy of the particle.

Consider first the effect of varying the cutoff distance, $x_{\rm cutoff}$. As mentioned above, this distance is chosen as a function of the initial width, as $x_{\rm cutoff} = x_0 + N\sigma_0$. To avoid some arbitrariness in the choice of N and ensure $\rho_0(x)$ vanishes far away from $x_{\rm cutoff}$, we define the ratio

$$\Gamma(x_{\rm cutoff}) \equiv \frac{\rho_0(x_{\rm cutoff})}{\rho_0(x_0)} = 10^{-n} \tag{35}$$

and call the exponent n the *sensitivity parameter*, which provides us with a minimum bond for the probability density (relative to its maximum value at the center of the initial wave packet). For example, setting $n = 6$ means that whenever $\Gamma(x(0)) < \Gamma(x_{\rm cutoff}) = 10^{-6}$, the probability density will be assumed to be zero (i.e., no probability below that value will be detected or computed). Accordingly, we have $N = \sqrt{2n \ln 10} \approx 2.15\, n^{1/2}$. In figure 2(a) we plot $x_{\rm cutoff}$ (dashed lines) and the corresponding curve $x_0^{\rm min}$ (solid lines) as a function of σ_0 for four different values of the sensitivity parameter: $n = 4$ (green), $n = 5$ (blue), $n = 6$ (purple) and $n = 7$ (red). As it can be noticed, as n increases, $x_0^{\rm min}$ also increases, which means to move the integration range in (13) towards regions with lower values of $\rho_0(x)$, this leading to smaller transmissions (see figure 2(b)). Nonetheless, the most important changes in the integration range happen at high values of σ_0, near the onset of no tunneling, this being the reason why in figure 2(b) there is only a difference $\mathcal{T}_\infty(n=4) - \mathcal{T}_\infty(n=7) \sim 0.0336$ ($\sim 6.72\%$ when this difference is referred to 0.5, the maximum value of $\mathcal{T}_\infty$) between the curves for $n = 4$ and $n = 7$, at $\sigma_0 \approx 0.138$ (see the position of the vertical dashed line). In figure 2(a) we have also plotted δ_0^c (black dashed-dotted line), which does not depend on the sensitivity parameter.

In the central part of figure 2 the effects of the slope of the potential on tunneling are displayed for three different values of the dynamical acceleration: $\alpha = 5$ (green), $\alpha = 10$ (blue) and $\alpha = 20$ (red). In all cases, the cutoff corresponds to a sensitivity parameter $n = 6$, with the black solid line of figure 2(c) denoting the position of $x_{\rm cutoff}$ for each value of σ_0. In figure 2(c), for the same value of α, solid lines indicate the position of $x_0^{\rm min}$ and dashed ones the position of δ_0^c. As the barrier slope α increases, tunneling probability decreases (see figure 2(d)). This decrease is again due to shift of the boundary curve δ_0^c when α increases, which leads to a smaller area between $x_{\rm cutoff}$ and $x_0^{\rm min}$ as well as to areas where the value of ρ_0 becomes meaningless (see below). Taking this fact into account, we can distinguish between two limits of interest. In the case of $\alpha \to \infty$, i.e., a vertical, infinite wall, no particle will be able to pass the barrier. On the contrary, when $\alpha \to 0$ and we have a flat surface, only half the number of particles from the initial ensemble are going to pass the barrier. In this latter case, the maximum value of $\mathcal{T}_\infty$ is only 0.5 because, as can be easily noted, $x_{\rm cl} = 0$ and,

¶ In all the calculations presented here, $\hbar = m = 1$. Moreover, when necessary, quantum trajectories have been calculated using standard wave packet propagation techniques [44] to obtain the wave function and then integrating (8).

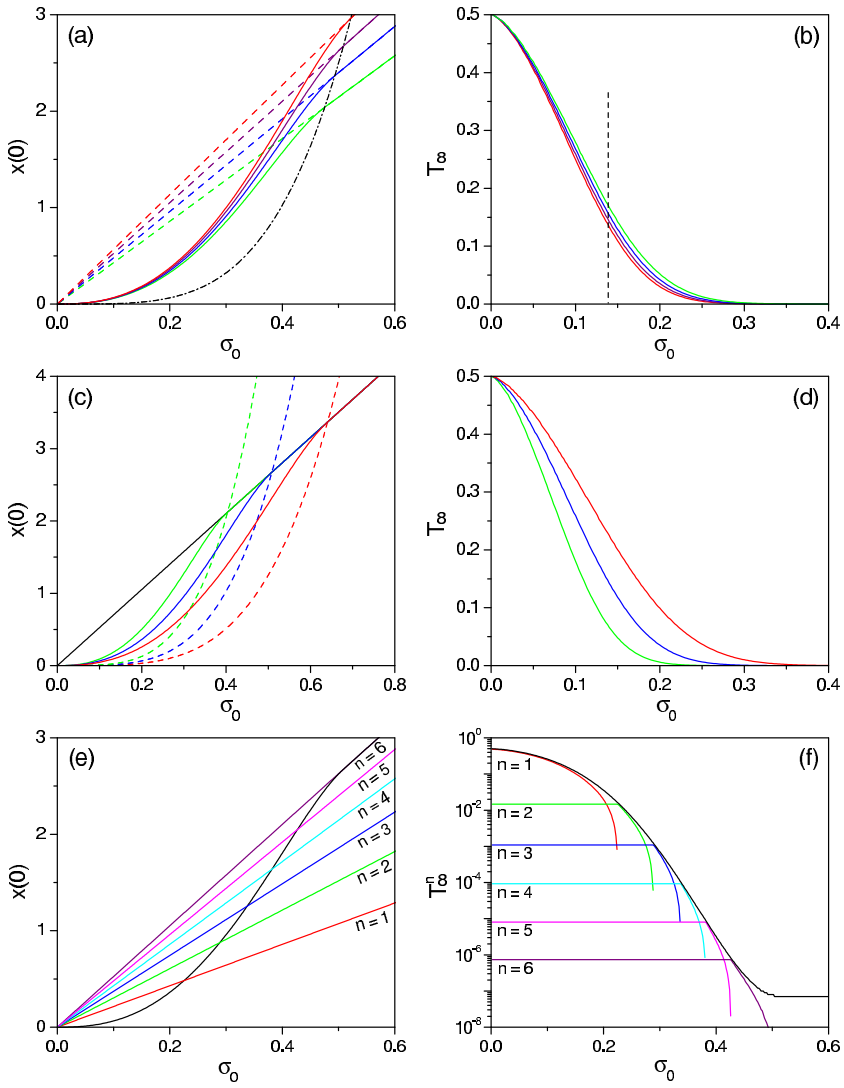

Figure 2. Top: $\mathcal{T}_\infty$ as a function of σ_0 for different values of the sensitivity parameter n and, therefore, of the cutoff position $x_{\rm cutoff}$: $n = 4$ (green), $n = 5$ (blue), $n = 6$ (purple) and $n = 7$ (red). In part (a), scheme to choose the initial positions, $x(0)$, for the calculation of $\mathcal{T}_\infty$ in panel (b): the cutoff position, $x_{\rm cutoff}$, is indicated by the dashed lines, $x_0^{\rm min}$ by the solid lines and δ_0^c by the black dashed-dotted line. Center: $\mathcal{T}_\infty$ as a function of σ_0 for different values of the barrier slope: $\alpha = 5$ (green), $\alpha = 10$ (blue) and $\alpha = 20$ (red). In part (c), scheme to choose the initial positions, $x(0)$, for the calculation of $\mathcal{T}_\infty$ in panel (d): the cutoff position, $x_{\rm cutoff}$, is indicated by the black solid line, $x_0^{\rm min}$ by the colored solid lines and δ_0^c by the colored dashed-dotted line. Bottom: Contributions to $\mathcal{T}_\infty$ from regions with different sensitivity range (see text for details). In part (e), $x_0^{\rm min}$ is indicated by the thick solid line, while the straight lines indicate limit of regions with sensitivities up to the value given in the corresponding label. In part (f), the thick solid line indicates $\mathcal{T}_\infty$, while the colored lines indicate indicate the contributions between two consecutive sensitivity values; each color corresponds to the upper sensitivity considered from part (e).

therefore, half of the particles will move forward (those starting in the front part of the wave packet, for which $\delta_0 > 0$) and another half will move backward (those from the rear part of the wave packet, with $\delta_0 < 0$).

To understand the different contributions of the region bounded between $x_{\rm cutoff}$ and $x_0^{\rm min}$ and therefore their role in the tunneling process, in the bottom part of figure 2 $\mathcal{T}_\infty$ is plotted as a function of different sensitivity parameters. In figure 2(e), we have plotted $x_0^{\rm min}$ (thick black line) for $\alpha = 10$ and a sensitivity of $n = 6$ (purple line). The positions of $x_{\rm cutoff}$ for different sensitivities are also plotted. These additional lines indicate that if $n = 2$ (green line), for example, the initial conditions lying between this line and $x_0^{\rm min}$ will give rise to probabilities such that $\Gamma(x(0)) \geq 10^{-2}$. The contribution $\mathcal{T}_\infty^n$ to the transmitted probability of initial conditions lying between two consecutive sensitivities $n-1$ and n is represented in figure 2(f); $\mathcal{T}_\infty$ is denoted with thick black line and labels indicate the cutoff chosen, e.g., $n = 2$ (green line) represents $\mathcal{T}_\infty^2$ from trajectories starting between the cutoffs with sensitivities $n = 1$ and $n = 2$ (the red and green lines in figure 2(e)). As can be seen, the most important contribution (almost 100%) arises from trajectories starting between $x_0^{\rm min}$ and $n = 1$, while as n increases the contributions decrease in about one order of magnitude and are only relevant as σ_0 increases.

3.2. Quantum trajectories and transmission probability

The results shown above provide us with valuable information concerning tunneling, although one can go a step further away yet. In figure 3 different sets of quantum trajectories are displayed in terms of σ_0. Thus, from top to bottom: $\sigma_0^{(1)} = 0.15$ (upper row), $\sigma_0^{(2)} = 0.3$ (middle row) and $\sigma_0^{(3)} = 0.5$ (lower row), which correspond (see figure 2(e)) to fast (strong), medium and slow (weak) boosting phases, respectively. In all cases, $x_0 = 0$, $v_0 = 0$ and $\alpha = 10$. Moreover, for computational convenience, we have considered a potential function

$$V(x) = \begin{cases} V_0 & x < x_- \\ m\alpha x & x_- \leq x \leq x_{\rm cutoff} \\ V_0 & x > x_{\rm cutoff} \end{cases} , \tag{36}$$

where $V_0 = m\alpha(x_0 - 3N\sigma_0)$ and $N = 5.26$, which corresponds to $n = 6$. The left-hand side truncation of the ramp avoids the increase of downhill velocity of the wave packet; to minimize effects due to the reflections induced by this change of slope [25, 26], we have assumed $x_- = x_0 - 3N\sigma_0$.

In figure 3(a) we notice that the fast or strong boosting ($\sigma_0 = \sigma_0^{(1)}$) provokes an almost immediate pushing of some trajectories in the opposite direction to the evolution of the center of the wave packet (thicker red line). In this case, the expansion of the wave packet is such that at $t = 1$ its width has increased more than 20 times σ_0, which is more than enough for an important number of trajectories to overcome the barrier (see figure 3(b)). From a standard quantum perspective (see figure 3(c)), the very narrow initial wave packet (black) passes to a very wide final one (blue dashed line), which splits into a reflected and a transmitted wave packet (blue solid lines) when the cutoff is considered (vertical green dashed line). For a weaker boosting (middle row), the width of the wave packet at $t = 1$ is about $5.6\sigma_0$ (see figure 3(d)). Meanwhile, the cutoff is at $x_{\rm cutoff} \approx 1.6$, which is only 3.5 times smaller than σ_t at $t = 1$. Thus, although some trajectories will be able to cross the barrier (see figure 3(e)), they start in regions where the initial probability density has small values and do not produce

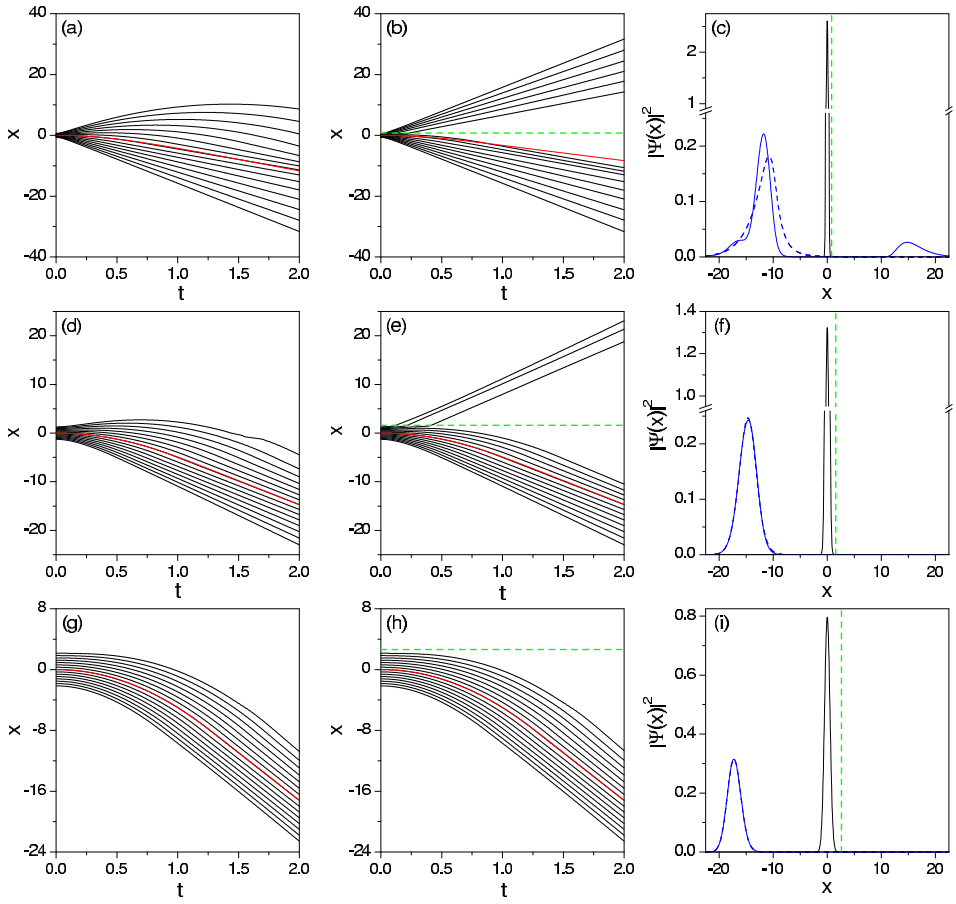

Figure 3. Quantum trajectories illustrating the collision dynamics with a linear, ramp-like potential (left-column panels) and the feasibility of tunneling when it is truncated (middle-column panels) for: $\sigma_0^{(1)} = 0.15$ (top row), $\sigma_0^{(2)} = 0.3$ (central row) and $\sigma_0^{(3)} = 0.5$ (bottom row). In each trajectory plot, the thick red curve indicates the average or expectation value of the position of the wave packet, $\langle \hat{x} \rangle$, with time. The position of $x_{\rm cutoff}$ for the corresponding value of σ_0 is shown by the dashed green line (horizontal in the middle-column panels and vertical in the right-column ones). In the right-column panels, from top to bottom, the initial (black line) and final (blue line) probability densities corresponding to each value of σ_0 are displayed. In these panels, final probability densities are plotted with solid line for the truncated potential and dashed line for the linear, ramp-like one.

much transmission. As seen in figure 3(f), transmission is almost negligible (about 500 times smaller than reflection). Finally, in the lower row of figure 3, a case of slow or weak boosting where quantum trajectories are out of the conditions leading to tunneling is displayed (see figure 2(e)) —the width of the wave packet here is about 2.2 times its initial width at $t = 1$, which is smaller than $x_{\rm cutoff}$. This is apparent in figure 3(h), where there are not transmitted trajectories, and also in Fig. 3(i), where there is no transmitted wave packet.

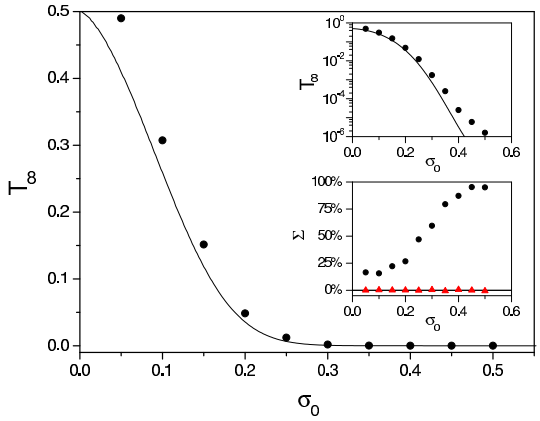

Figure 4. Transmission probability, $\mathcal{T}_\infty$, as a function of the initial width of the wave packet estimated with (19) and (24) ($\mathcal{T}_\infty^{est}$, solid line) and obtained from a wave packet simulation ($\mathcal{T}_\infty^{wp}$, circles) for several values of σ_0. In the upper inset, the same plot but at a logarithmic scale to show the discrepancy between both calculations as σ_0 increases. In the lower inset, deviation Σ (see text for details) for the estimated values (black circles) and the corrected ones (red triangles) with respect to the values obtained from the wave packet simulation. The values of the parameters considered are: $\alpha = 10$, $x_0 = 0$ and $v_0 = 0$.

Finally, in figure 4 we have plotted $\mathcal{T}_\infty$ when it is estimated with the previous simple model ($\mathcal{T}_\infty^{est}$, solid line) and also from wave packet calculations ($\mathcal{T}_\infty^{wp}$, black circles) —using quantum trajectories sampled according to ρ_0 would render exactly the same results, as shown elsewhere [39]. As can be noticed, though the estimated transmission $\mathcal{T}_\infty^{est}$ follows very nicely the trend of the correct value, $\mathcal{T}_\infty^{wp}$, there is a discrepancy between both magnitudes which increases with σ_0. This can be better appreciated in the upper inset of the figure, where the $\mathcal{T}_\infty$ axis is given in logarithmic scale, as well as in the lower inset, where the deviation between both values (measured in percentages, %),

$$\Sigma \equiv \left(1 - \frac{\mathcal{T}_\infty^{est}}{\mathcal{T}_\infty^{wp}}\right) \times 100\%. \tag{37}$$

is calculated. In order to understand these deviations, in figures 2(e) and 2(f) we see that, given σ_0, those trajectories started between the (red) line for $n = 1$ and $x_0^{\min}$ would be the ones with a larger contribution (the following, between $n = 1$ and $n = 2$, contribute with a probability almost two orders of magnitude smaller). Thus, note that, beyond $\sigma_0 \approx 0.225$ the probabilities are very low (see green curve in figure 2(f)) and, therefore, small variations in the position of $x_{\min}$ may imply larger relative errors, as can be seen in the lower inset of figure 4. Now, the source for these deviations arises from the fact that, in the model considered here, $x_0^{\min}$ was chosen assuming that the last trajectory penetrating into the transmission region coincides with x_{cutoff}. This implies to neglect all those trajectories whose turning points are very close to x_{cutoff}, but without touching it (i.e., with $x(0) \lesssim x_0^{\min}$). Thus, provided they are in a neighborhood of x_{cutoff}, the corresponding trajectories should also be taken into account and the $x_0^{\min}$ curve should be correspondingly corrected. If we use the trajectory plots to determine the initial position of the boundary trajectory, and consider it to estimate again $\mathcal{T}_\infty$ through (19) but with the new $x_0^{\min}$ positions,

effectively, we obtain $\mathcal{T}_{\infty}^{wp}$, as indicated by the red triangles in the lower panel of figure 4. In order to appreciate the importance of a good characterization of the region of initial conditions leading to tunneling, consider, for example, $\sigma_0 = 0.15$. In this case, $x_0^{min,\ est} \approx 0.1774$ and $\mathcal{T}_{\infty}^{est} \approx 0.11795$. However, when we localize the initial position of the boundary trajectory, $x_0^{min,\ corr} \approx 0.1547$, and correct accordingly the lower value of initial positions, we obtain $\mathcal{T}_{\infty}^{corr} \approx 0.15149$, which is very close to the value obtained from the simulation, $\mathcal{T}_{\infty}^{wp} \approx 0.15149$. Thus, a displacement $x_0^{min,\ est} - x_0^{min,\ corr} \approx 0.0227$ in an interval $x_0^{\rm cutoff} - x_0^{min,\ corr} \approx 0.6328$ leads to a decrease of the true transmission probability of about 22%, while the corrected one differs only in about a 0.03% (both value are obtained using (37)). Now, if we proceed similarly with $\sigma_0 = 0.3$, we find $x_0^{min,\ est} - x_0^{min,\ corr} \approx 0.0823$ in an interval $x_0^{\rm cutoff} - x_0^{min,\ corr} \approx 0.7024$. This leads to a decrease of the true transmission probability of about 60%, while the corrected one differs only less than 0.5%.

4. Conclusions

Usually in standard quantum mechanics, the transmission or tunneling probability is associated with the height and width of a barrier. Analytical expressions for this probability can be derived from time-independent or semi-classical calculations [25, 26] after setting some matching conditions on both the wave function and its first derivative at the barrier edges. On the other hand, from a numerical viewpoint, transmission probabilities are usually obtained from wave packet calculations, computing the amount of transmitted probability accumulated beyond a certain boundary [20].

A complementary and alternative way to look at tunneling readily arises when Bohmian mechanics is considered. In principle, this approach helps us to discern which part of the incident wave packet is transmitted through the barrier and how this takes place by monitoring the trajectory flow along time. However, as we have shown here, one can go beyond these facts and determine tunneling conditions by studying the individual behavior of quantum trajectories, which can be used in a practical way to obtain fair estimates of transmission probabilities with information only related to the system initial state, according to the general result (13). To illustrate this interesting fact, we have considered the collision of a Gaussian wave packet with a ramp-like barrier, for which (13) can be recast as in the form given by (19). This general expression for Gaussian wave packets presents some remarkable properties. First, tunneling can be explained essentially in terms of three physical (measurable) parameters: the wave packet motion (through v_0), the wave packet spreading (through σ_t and therefore v_s) and the barrier slope (through α). This arises through the estimates of $x_0^{\rm min}$, according to expressions like (24), (30) or (34). Second, once $x_0^{\rm min}$ is set up, (19) allows us to estimate and compute transmission probabilities. Third, conversely, given the transmission probability the inverse procedure can be used to determine the dynamical boundaries of the wave packet that lead to tunneling, which can be used to extract valuable information about the physical properties associated with the wave packet or the barrier (using expressions like (24), (30) or (34)).

Based on the aforementioned properties, in our opinion, the study presented here constitutes an important resource at an applied level. Despite that quantum trajectories are not experimentally observable, the information they provide can be seen as a tool to analyze experimental processes and phenomena where tunneling

is involved. In particular, it could be employed to understand and implement mechanisms aimed at quantum controlling molecular systems, alternative to (or cooperative with) other mechanisms proposed in the literature [45–51], since the treatment here described stresses a direct relationship between the experimental effect (tunneling) and the initial state. In virtue of this relationship, fairly well summarized by (13) or its Gaussian version, (19), one could control the further state of the system (i.e., the occurrence of tunneling) by selecting different values of the parameters involved in the preparation of the initial state (i.e., the initial conditions of the Gaussian wave packet).

Acknowledgments

Support from the Ministerio de Ciencia e Innovación (Spain) under Projects FIS2010-18132 and FIS2010-22082 is acknowledged. A. S. Sanz would also like to thank the same Institution for a "Ramón y Cajal" Research Fellowship.

References

[1] Main I G 1993 *Vibrations and Waves in Physics* 3rd edn (Cambridge: Cambridge University Press)
[2] Born M and Wolf E 1999 *Principles of Optics* 7th edn (Cambridge: Cambridge University Press)
[3] Fowler R H and Nordheim L W 1928 *Proc. R. Soc.* A **119** 173
[4] Gamow G 1928 *Z. Phys.* **51** 204
[5] Gurney R W and Condon E U 1928 *Nature* **122** 439
[6] Wood R W 1897 *Phys. Rev.* **5** 1
[7] Elster J and Geitel H F 1899 *Verh. Dtsch. Phys. Ges.* **1** 136
[8] Razavy M 2003 *Quantum Theory of Tunneling* (River Edge, NJ: World Scientific)
[9] Ankerhold J 2007 *Quantum Tunneling in Complex Systems (Springer Tracts in Modern Physics* vol 224*)* (New York: Springer)
[10] Zang D H and Pollak E 2004 *Phys. Rev. Lett.* **93** 140401
[11] Bohm D 1952 *Phys. Rev.* **85** 166, 180
[12] Holland P R 1993 *The Quantum Theory of Motion* (Cambridge: Cambridge University Press)
[13] Hirschfelder J O, Christoph A C and Palke W E 1974 *J. Chem. Phys.* **61** 5435
[14] Dewdney C and Hiley B J 1982 *Found. Phys.* **12** 27
[15] Goldberg A, Schey H M and Schwarts J L 1967 *Am. J. Phys.* **35** 177
[16] Lopreore C L and Wyatt R E 1999 *Phys. Rev. Lett.* **82** 5190
[17] Wyatt R E 1999 *J. Chem. Phys.* **111** 4406
[18] Wyatt R E 2005 *Quantum Dynamics with Trajectories* (New York: Springer)
[19] Madelung E 1926 *Z. Phys.* **40**, 322
[20] Sanz A S, Giménez X, Bofill J M and Miret-Artés S 2009 *Chem. Phys. Lett.* **478** 89
Sanz A S, Giménez X, Bofill J M and Miret-Artés S 2010 *Chem. Phys. Lett.* **488** 235 (erratum)
[21] Sanz A S, Davidović M, Božić and Miret-Artés S 2010 *Ann. Phys.* **325** 763
[22] Kocsis S, Braverman B, Ravets S, Stevens M J, Mirin R P, Shalm L K and Steinberg A M 2011 *Science* **332** 1170
[23] Leavens C R 2008 Bohm trajectory approach to timing electrons *Time in Quantum Mechanics (Lecture Notes in Physics* vol 734*)* ed G Muga, R Sala-Mayato and I Egusquiza (Berlin: Springer)
[24] Fleurov V and Soffer A 2005 *Europhys. Lett.* **72** 287
[25] Schiff L I 1968 *Quantum Mechanics* (Singapore: McGraw-Hill) 3rd ed
[26] Liboff R L 1980 *Introductory Quantum Mechanics* (Reading, MA: Addison-Wesley)
[27] Sanz A S and Miret-Artés S 2008 *J. Phys. A* **41** 435303
[28] Berry M V and Balazs N L 1979 *Am. J. Phys.* **47** 264
[29] Unnikrishnan K and Rau A R P 1996 *Am. J. Phys.* **64** 1034
[30] Siviloglou G A, Broky J, Dogariu A and Christodoulides D N 2007 *Phys. Rev. Lett.* **99** 213901
[31] Sanz A S 2005 *J. Phys. A* **38** 6037
[32] Sanz A S and Miret-Artés S 2007 *J. Chem. Phys.* **126** 234106

[33] Chou C-C, Sanz A S, Miret-Artés S and Wyatt R E 2009 *Phys. Rev. Lett.* **102** 250401
Chou C-C, Sanz A S, Miret-Artés S and Wyatt R E 2010 *Ann. Phys.* **325** 2193
[34] Heller E J 1975 *J. Chem. Phys.* **62** 1544
[35] Tannor D J 2007 *Introduction to Quantum Mechanics. A Time-Dependent Perspective* (Sausalito, CA: University Science Books)
[36] Sanz A S, López-Durán D and González-Lezana T 2011 *Chem. Phys.* (at press) doi:10.1016/j.chemphys.2011.07.017
[37] Sanz A S and Miret-Artés S 2005 *J. Chem. Phys.* **122** 014702
[38] Brumer P and Jiangbin G 2006 *Phys. Rev. A* **73** 052109
[39] Sanz A S, Borondo F and Miret-Artés S 2000 *Phys. Rev. B* **61** 7743
[40] Sanz A S, Borondo F and Miret-Artés S 2002 *J. Phys.: Condens. Matter* **14** 6109
[41] Abramowitz M and Stegun I A (eds) 1972 *Handbook of Mathematical Functions with Formulas, Graphs and Mathematical Tables* (New York: Dover) chapter 7
[42] Nickalls R W D 2009 *Math. Gaz.* **93** 66 http://www.nickalls.org/dick/papers/maths/quartic2009.pdf
[43] Nickalls R W D 1993 *Math. Gaz.* **77** 354 http://www.nickalls.org/dick/papers/maths/cubic1993.pdf
[44] Sanz A S and Miret-Artés 2007 *Phys. Rep.* **451** 37
[45] Grossman F, Dittrich T, Jung P and Hänggi P 1991 *Phys. Rev. Lett.* **67** 516
[46] Rego L G D, Abuabara S G and Batista V S 2006 *J. Mod. Opt.* **53** 2519
[47] Lignier H, Sias C, Ciampini D, Singh Y, Zenesini A, Morsch O and Arimondo E 2007 *Phys. Rev. Lett.* **99** 220403
[48] Arimondo E and Wimberger S 2011 Tunneling of ultracold atoms in time-independent potentials *Dynamical Tunneling: Theory and Experiment* ed S Keshavamurthy and P Schlagheck (New York: CRC Press) pp 257-87
[49] Ohmura H and Tachiya M 2008 *Phys. Rev. A* **77** 023408
[50] Ohmura H, Saito N and Morishita T 2011 *Phys. Rev. A* **83** 063407
[51] Lu G, Hai W and Xie Q 2011 *Phys. Rev. A* **83** 013407